Phase calibration of spatially nonuniform spatial light modulators

Xiaodong Xun and Robert W. Cohn

A new 512 × 512 pixel phase-only spatial light modulator (SLM) has been found to deviate from being flat by several wavelengths. Also, the retardation of the SLM relative to voltage varies across the device by as much as 0.25 wavelength. The birefringence of each pixel as a function of address voltage is measured from the intensity of the SLM between crossed polarizers. To these responses are added a reference spatial phase measured by phase shifting interferometry for a single address voltage. Fits to the measured data facilitate the compensation of the SLM to a root-mean-square wave-front error of 0.06 wavelength. The application of these corrections to flatten the full aperture of the SLM sharpens the focal plane spot and reduces the distortion of computer-designed diffraction patterns. © 2004 Optical Society of America

OCIS codes: 230.6120, 050.1970, 070.2580, 120.5050, 120.3180.

1. Introduction

Electrically addressed, phase-only spatial light modulators (SLMs) are usually calibrated to correct for the nonlinear mapping of voltage (or digital gray-scale level) to phase modulation.[1] For many of the reported calibration methods it has been assumed that the SLM is spatially uniform in phase and in responsiveness (i.e., the phase-versus-voltage response). If the SLM is uniform, the phase shift can be determined in the modulation plane from a shift in fringe position when a reference wave interferes with a plane wave transmitted through or reflected from the SLM[1–4] or in the Fourier plane from the interference between the SLM diffraction pattern and a reference wave (in some cases from an unmodulated portion of the SLM).[5–7] For SLMs that are based on electro-optic modulation of birefringence, most notably parallel-aligned liquid-crystal SLMs, the phase shift can be directly determined also from the intensity modulation caused by the combination of the SLM (illuminated with linear polarization at −45° from the ordinary and extraordinary axes) and an analyzer polarizer (at a cross-polarization angle +45° from the extraordinary axis).[8]

The authors are with the ElectroOptics Research Institute and Nanotechnology Center, University of Louisville, Louisville, Kentucky 40292. R. W. Cohn's e-mail address is rwcohn@uofl.edu.

Received 7 July 2004; revised manuscript received 14 September 2004; accepted 15 September 2004.

0003-6935/04/356400-07$15.00/0

However, we recently began using a prototype liquid-crystal SLM that is spatially nonuniform at a single phase setting and (to a lesser degree) is spatially nonuniform in its phase-versus-voltage response.[9,10] The nonuniformity is due to curvature of the SLM's backplane addressing circuit that results from differences in polishing rates between metalized and nonmetalized regions of the backplane.[11] We measured the resultant phase characteristics and then compensated for them to achieve diffraction patterns that one would expect from a nominally flat SLM.

By way of introduction, we show in Figs. 1(a)–1(c) that, at a constant gray level, setting the SLM produces a nonuniform spatial distribution that is rectangularly symmetric (owing to polishing of the rectangularly diced backplane chip[11]). Whereas a spherical phase error could be compensated for in a Fourier diffraction pattern by a shift in the focal plane, the rectangular shape will cause distortion of the diffraction pattern. Figure 1 also shows that the SLM phase [Fig. 1(b)] (which is visualized as an interference pattern with a flatter than λ/10 reference mirror) is not simply related to the birefringence of the SLM as viewed through a polarization analyzer [Fig. 1(c)]. Furthermore, the cover glass of the SLM produces a different interference pattern with the backplane [Fig. 1(a)] from that produced by the reference mirror. The nonequivalence of phase and birefringence is even more clearly seen when one compensates for the phase [Fig. 1(e)] and views the birefringence through an analyzer [Fig. 1(f)]. The compensation includes correction for nonuniform responsiveness as well. These results make clear that, when the SLM is used as a

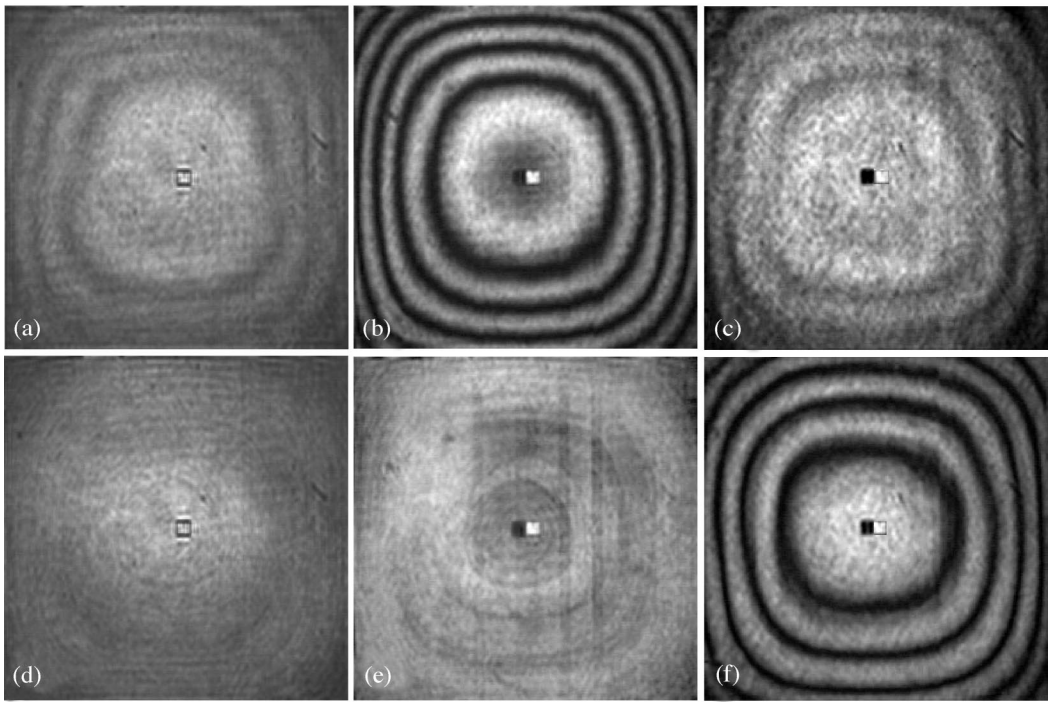

Fig. 1. Intensity images of the SLM illuminated by a collimated laser beam. (a)–(c) The SLM is addressed with a constant gray-scale voltage; (d)–(f) the SLM is calibrated to produce a spatially uniform phase. (a), (d) Intensity images of the SLM. Intensity variations are due to interference between the liquid-crystal layer and the cover glass, to nonuniform intensity of the collimated beam, and to high spatial frequency of the SLM phase modulation. (b), (e) Interferograms of the SLM with a flat reference mirror. (c), (f) SLM viewed through crossed polarizers at $\pm 45°$ to the extraordinary axis of the SLM. The small blocks in the center of each image have been experimentally adjusted to provide references for maximum and minimum brightness.

programmable phase-only diffraction grating, its phase must be directly measured.

We attempted several approaches to calibration, finally settling on one in which we minimized drift and vibration errors in interferometric measurements by gathering the phase data as quickly as possible. Specifically, the spatial phase at a single gray-level setting of the SLM is measured by phase-shift interferometry (which can drift substantially over even a few seconds), and then the change in intensity caused by a change in birefringence as a function of gray scale is measured through crossed polarizers (which are quite insensitive to vibration). For the specific characteristics of the SLMs studied (which are essentially linear over one wavelength of retardation) a relatively small amount of calibration data (reference phase and phase shift per gray level) needs to be stored to run the calibration algorithm.

In the remainder of this paper we report, in sequence, the measurement procedure, specific measurements of the nonuniformity of the modulation, a description of the compensation method, and experimental demonstrations of the resultant improvements in the modulator plane and the diffraction plane.

2. Spatial Light Modulator and Measurement Apparatus

A model 512N15-532 (Boulder Nonlinear Systems, Inc., Lafayette, Colorado) reflective SLM is used in this study. It is filled with parallel-aligned nematic liquid crystals and has 512×512 square pixels on a pitch of 15 μm.[10] The SLM is addressed with 128 gray-scale levels. The SLM's characteristics are measured in the setup shown in Fig. 2. The system as shown can be configured to record the diffraction pattern at the focal plane of the output lens (120-mm focal length) or the image of the SLM at the image plane.

A reference piezo mirror (flatter than $0.1\ \lambda/25$ mm at wavelength $\lambda = 532$ nm) is introduced to record interferograms and measure phase by phase-shift interferometry. A four-phase phase-shift interferometry algorithm is used in which the reference piezo mirror is shifted in four $\lambda/4$ steps (typically in our measurements at 0.25 s/step) to produce four interferogram intensity patterns (I_1, I_2, I_3, and I_4).[12] The interferograms are recorded by a black-and-white video CCD camera and digitized by a frame grabber. The phase at a specific pixel location in intensity images is evaluated as

$$\phi = \tan^{-1} \frac{I_4 - I_2}{I_1 - I_3}. \tag{1}$$

The polarization of the laser (a diode-pumped 532-nm Nd:YVO_4 laser) is along the extraordinary axis of the liquid crystal. The system also includes two polarizers, which are aligned with the extraordinary axis of the liquid crystal (to remove residual polarizations) for phase measurements and diffraction-pattern generation and which are rotated

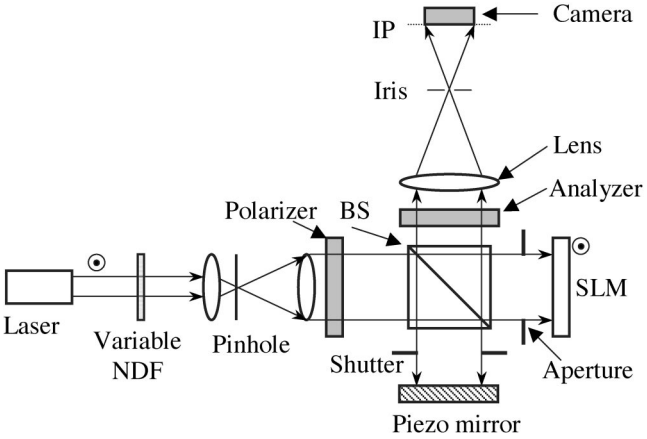

Fig. 2. Schematic of the SLM phase-measurement system (top view). The desired interferogram between the SLM and the piezo mirror is formed on the camera when both polarizers and the laser are polarized along the extraordinary axis of the SLM [e.g., as in Fig. 1(b)]. Ideally, no intensity variation is seen when the shutter is closed in front of the piezo mirror [e.g., as in Fig. 1(a)]. With the shutter closed, the intensity variations that are due to spatially varying birefringence are seen when the polarizers are at $\pm 45°$ to the extraordinary axis [e.g., as in Fig. 1(f)]. NDF, neutral-density filter; BS, beam splitter; IP, image plane.

to $-45°$ and $+45°$ from the extraordinary axis for intensity imaging of the electro-optic retardation of the liquid crystal.

The intensity variation for a parallel-aligned liquid crystal is

$$I = I_0(1 + \cos \phi)/2, \tag{2}$$

where

$$\phi = 2\pi(n_e - n_o)l/\lambda \tag{3}$$

is the difference in phase retardation between the extraordinary and the ordinary axes, l is the path length (twice the thickness of the liquid crystal in the reflective SLM), and λ is the wavelength of light. A continuous sweep of the addressing voltage permits an unambiguous determination of the phase retardation as a function of gray scale. Note that we find it convenient to report spatial phase and phase retardation in units of wavelength or as an optical thickness, i.e.,

$$t = \phi/(2\pi), \tag{4}$$

where t is assumed to be in units of λ.

A neutral-density filter wheel is located immediately after the laser to adjust intensity on the CCD. As the SLM is only ~50% reflective, a neutral-density filter is used in front of the reference mirror to improve fringe contrast of the recorded images shown in the paper. However, the attenuator is removed during phase-shift interferometry. In all the reported experiments, both the interferograms and the polarization intensity images of the 512×512 SLM pixels are imaged to 250×250 pixels of the 640×480 pixel CCD. Frame grabber data are processed on a personal computer in a Labview (National Instruments, Austin, Texas) software environment configured with a combination of custom-written programs and built-in Labview functions.

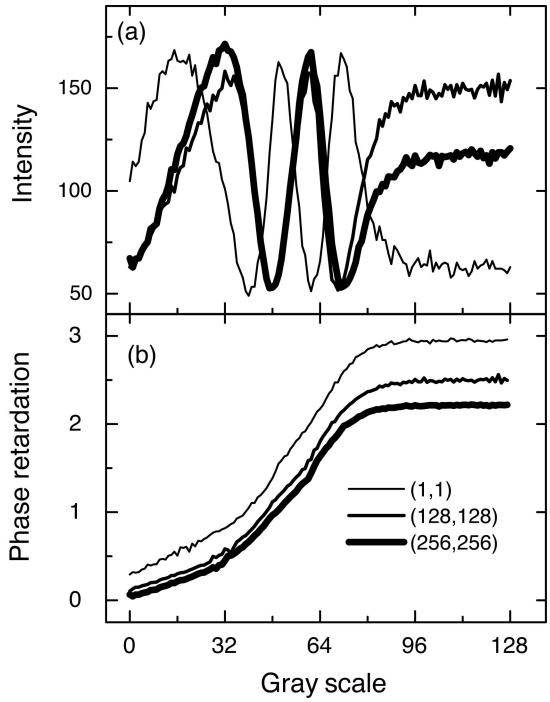

Fig. 3. Measurements of the SLM's change in birefringence as a function of gray-scale voltage at selected SLM pixels: corner (1, 1), halfway to the center (128, 128), and the center (256, 256). (a) Intensities recorded by the camera of the SLM between crossed polarizers. (b) Phase retardation calculated from (a).

3. Measurements of Retardation, Responsiveness, and Spatial Phase

A. Retardation and Responsiveness

We determine phase retardation as a function of address voltage (or responsiveness) for the SLM by measuring the intensity response for each pixel of the camera (corresponding to ~4 pixels of the SLM) and then determining the retardation by using Eqs. (2) and (3). Figure 3 shows the intensity and phase retardation responses for three camera pixels [near the corner (1, 1), halfway to the center (128, 128), and the center (256, 256)] of the SLM.

Several features of the SLM are notable. First, the SLMs retardation is nearly linear, with address voltage at least 1.5λ between gray-scale levels of 34 and 72. Second, at 0 gray-scale address voltage the regions differ in retardation by $\sim 0.13\lambda$, whereas at 128 gray scale the retardation differs by 0.45λ. In fact, the slope of the responsiveness δt varies across the device, with the greatest slope found for the pixels near the edge of the SLM. The slope of the linear retardation-versus-gray-scale region (as measured at gray-scale values of 34–72 over one wavelength of retardation) varies from $\delta t = \lambda/25$ per gray level (near the center) to $\lambda/20$ per gray level (at the corner

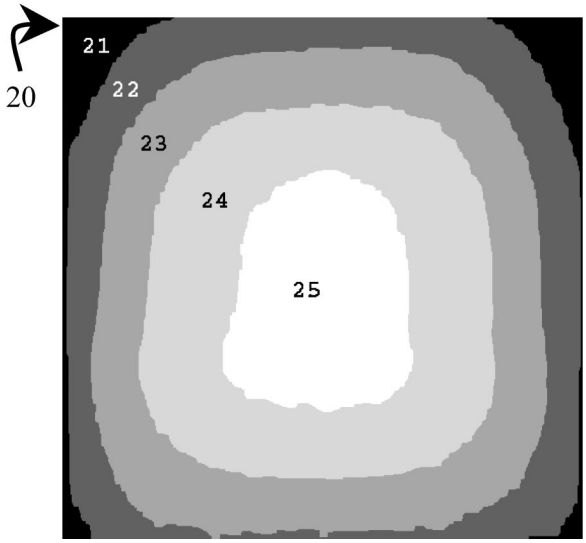

Fig. 4. Map of spatially varying phase responsiveness across the SLM. Depending on the location across the SLM, 20–25 gray-scale levels produce a 1λ retardation.

of the SLM). This variation in responsiveness is plotted in Fig. 4. The values were calculated by use of a Labview built-in function (Pulse measurements.vi) that measures the period of the intensity as a function of gray scale. The function returns the period as an integer. Whereas one could use regression analysis to obtain a noninteger period, the built-in function is preferred because of its computational speed over that of regression analysis. If the slope were treated as constant across the SLM, the corner pixels would be in error by as much as $\lambda/4$ (when the corner pixel is programmed for 1λ with the slope of the center pixel.) Taking the slope changes into account, one can reduce the error to residual rounding error (of the Labview built-in function), which (for this specific SLM) is $\lambda/20$ or less.

B. Spatial Phase

As discussed in Section 1, the phase retardation as measured between crossed polarizers does not provide spatial phase when the SLM is not flat and its optical surface is unknown. However, if the spatial phase distribution or optical thickness $t(x, y)$ (where x and y are the transverse coordinates) is known for one gray-scale setting, it can be used to establish a reference phase for the retardation-versus-gray-scale response of each pixel. Furthermore, if the SLM's phase-versus-gray-scale response is linear, the spatial phase distribution for any array of gray-scale settings $V(x, y)$ can be expressed as

$$t(x, y) = t_0(x, y) + \delta t(x, y)[V(x, y) - V_0], \quad (5)$$

where $t_0(x, y)$ is the optical thickness function measured at gray-scale setting V_0. We find that every pixel of our SLM is reasonably linear (over at least 1λ) for a reference gray-scale value of $V_0 = 44$.

Intensity images similar to those in Fig. 1(b) were collected for four reference phases for a gray-scale value of $V_0 = 44$. Figure 5(a) shows the phase distribution for the SLM as measured by the phase-shift interferometry method of Section 2. The resultant curvature of the optical surface is quite large and slowly varying compared with the pixel spacing. It seems reasonable to assume that much of the noise in the phase image is a measurement artifact. Based on this assumption, we unwrapped the phase (with Labview function Unwrap Phase.vi), smoothed it with a Savitzky–Golay 5×5 two-dimensional filter, and rewrapped the data to produce the phase image in Fig. 5(b). The error between the two phase images is presented in Fig. 5(c) for comparison.

4. Calibrated Programming of the Spatial Light Modulator

One achieves a desired phase pattern $t(x, y)$ by supplying calibrated address voltages $V(x, y)$ to the SLM. These voltages are found by inversion of Eq. (5) to get

$$V(x, y) = V_0 + [t(x, y) - t_0(x, y)]/\delta t(x, y). \quad (6)$$

Although the equation is linear, it is possible that values of $V(x, y)$ lie outside the linear range of the modulator. This problem is simply handled by modeling the calibrated optical thickness $t(x, y) - t_0(x, y)$ from 0 to λ (i.e., modeling the phase from 0 to 2π).

As a test of the calibration, we programmed the SLM to constant optical thickness and then measured the phase of the SLM by phase-shift interferometry. The measured phase represents devi-

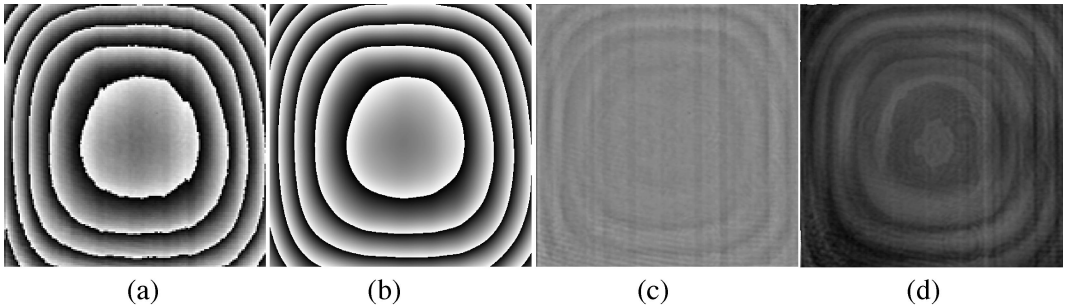

Fig. 5. (a) Measured and (b) smoothed phase distributions, and (c) the phase difference between (a) and (b) for gray-scale address voltage $V_0 = 44$. The rms phase difference for the entire image in (c) is 0.003λ. (d) Residual phase measured with the calibration in Figs. 4 and 5(b). The rms residual phase error in (d) is 0.06λ. (a)–(d) Black denotes 0λ and white denotes 1λ optical thickness.

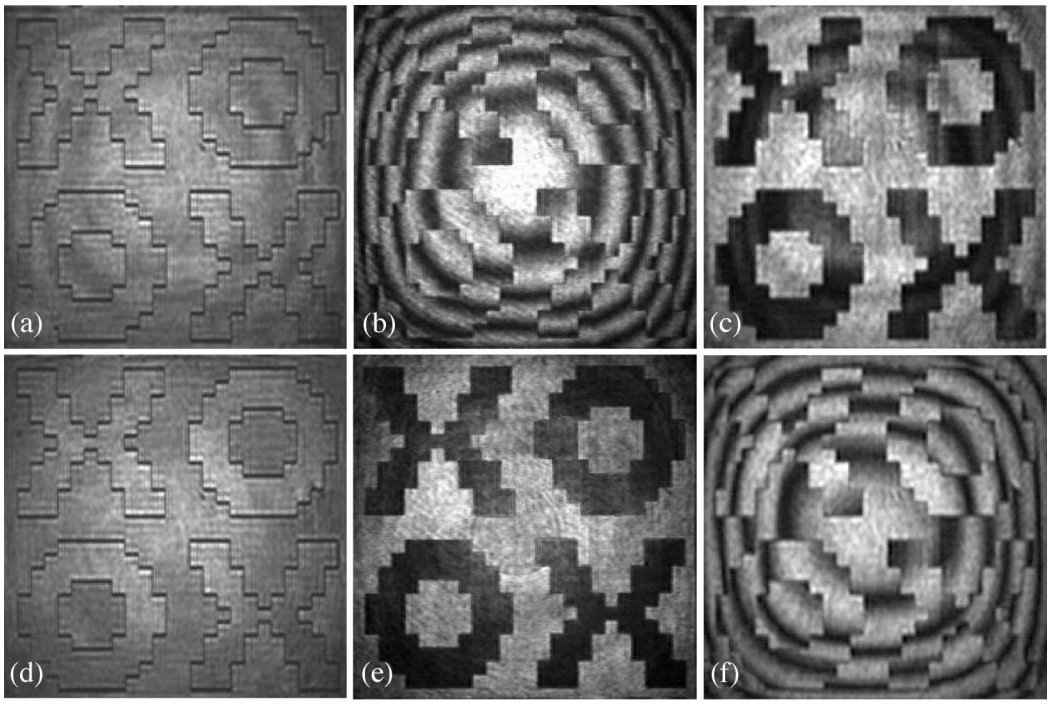

Fig. 6. Intensity images of the SLM loaded with a binary image (a)–(c) without and (d)–(f) with calibration. The SLM is illuminated identically as for Fig. 1, and the images are arranged identically to the images in Fig. 1. The designed retardations for the binary image are 0 and $\lambda/2$.

ations from perfect calibration. Figure 5(d) shows the wave-front errors for a thickness setting of $\lambda/4$. The curvature has mostly been canceled, but there is noticeable ripple in the image that appears most similar to the fringe pattern in Fig. 1(b). The root-mean-square (rms) wave-front error for this thickness setting is 0.06λ. The other thickness settings have similar values of rms wave-front error (e.g., 0.062λ and 0.058λ rms for thickness settings of 0λ and $\lambda/2$, respectively). Considering the magnitude of the interference fringes from cover glass reflections (which are not considered in the phase-shift interferometry algorithm), the quantization error (which is as large as 0.05λ), and other random and deterministic errors in the system, we consider the calibration reasonably good.

The usefulness and quality of the calibration are demonstrated by comparison of the interferograms in Figs. 6(b)–6(e). The image in Fig. 6(d) is reasonably well compensated to the casual observer. The corresponding images of the SLM viewed between crossed polarizers go from appearing mostly corrected in Fig. 6(c) to being quite curved in Fig. 6(f) after the phase is compensated for.

Another test of the calibration is to block the reference mirror and use the calibrated SLM as a phase-shift mirror that interferes (in line) with the cover glass. The resultant path differences (Fig. 7) are interpreted as a measure of the curvature of the cover glass, which for this SLM corresponds to more than 1λ optical path difference.

The calibration can be used to improve the quality of Fourier plane diffraction patterns, as is illustrated in Figs. 8 and 9. To separate the SLM impulse response from the on-axis spot caused by the reflection from the cover glass, the SLM is programmed with a linear phase ramp. With calibration the spot has narrower and lower sidelobes than without calibra-

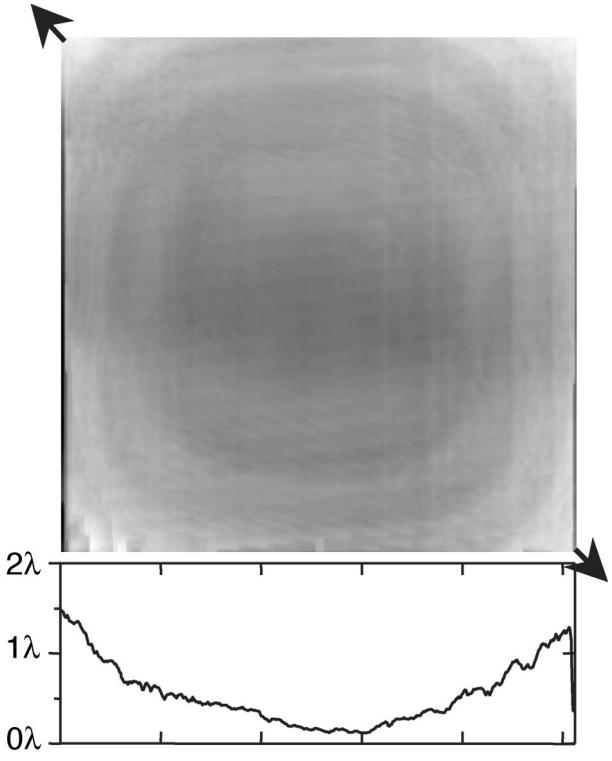

Fig. 7. Measured surface curvature of the cover glass. The cross section is that of the diagonal indicated by the two arrows.

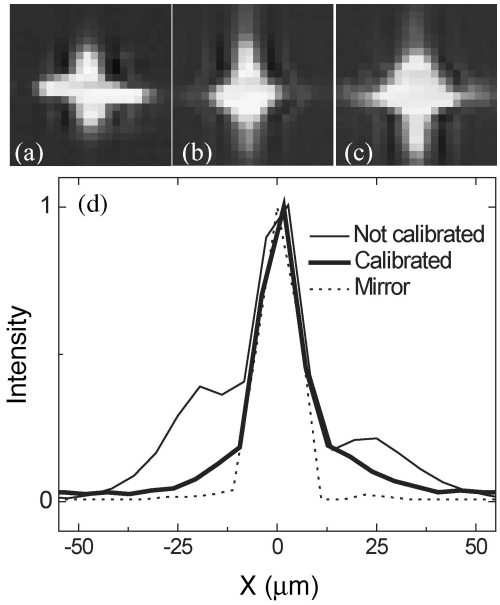

Fig. 8. Intensity distributions of the focal spot from the SLM (a) without and (b) with calibration. (c) Diffraction pattern from a mirror of the same aperture as the reflective SLM used in place of the SLM to estimate the diffraction limit. (d) Cross sections along the vertical center lines of (a)–(c). Spots in (a) and (b) were generated off axis to prevent on-axis reflection from the cover glass of the SLM. The lightest white in images in (a), (b), and (c) corresponds to 5%, 5%, and 2.5%, respectively, of the respective peak intensities of the spots.

tion (Fig. 8). One can compare the SLM with an ideally flat SLM by replacing the SLM with a mirror that has an aperture identical to the SLM. This experimental result for a mirror is shown in Figs. 8(c) and 8(d). For further comparison it should be noted that the diameter of this spot (full width at half-maximum) is within 5% of the diameter of the diffraction-limited spot (for a uniformly illuminated square aperture and a 120-mm focal-length lens.)

Figure 9 shows a second diffraction pattern of some complexity. The desired pattern consists of two spatially separated circular rings. A complex-valued modulation that will generate such a pattern is expressed as[13]

$$E = \exp\left[i2\pi\left(\frac{r}{r_1} + \frac{x+y}{S_1}\right)\right] + \exp\left[i2\pi\left(\frac{r}{r_2} + \frac{x+y}{S_2}\right)\right], \quad (7)$$

where x and y are the coordinates on the SLM plane that originated at the center, and $r = \sqrt{x^2 + y^2}$. The radius of the large ring is chosen as $r_1 = 32$, and the ring is shifted from the origin by $S_1 = 64$. For the small ring, $r_2 = 16$ and $S_2 = 128$. The amplitudes of the complex electric field are encoded onto a phase-only modulation by a minimum-distance pseudorandom encoding method.[14] The uncorrected modulation produces distorted rings, whereas the compensated modulation produces circular rings, as designed. Generally speaking, the SLM is successfully corrected for application as a programmable diffractive optic, bringing the performance of the SLM much closer to the diffraction limit than without the correction.

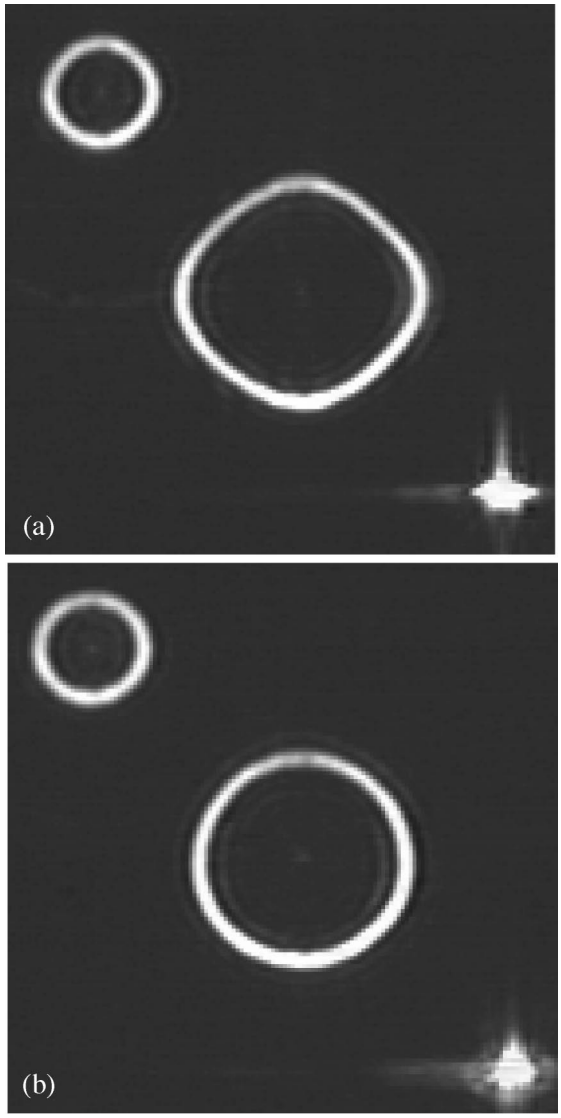

Fig. 9. Diffraction pattern of two rings produced by the SLM (a) without calibration and (b) with calibration.

5. Discussion and Summary

We have presented a phase-only SLM calibration procedure that combines the simple and robust measurement of retardation with crossed polarizers and a phase-shift interferometry measurement for a single gray-scale address voltage. This procedure facilitates compensation of nonflat SLMs for use as programmable diffractive optical elements. Corrections to 0.06λ rms were achieved for the reported SLM. We have also compensated two other SLMs of the same model, one at the same visible wavelength of 532 nm and the other at 1064 nm, with similar results. We used essentially identical hardware, including identical visible CCD cameras, and achieved

compensation of comparable quality. The calibrations for these SLMs were used in creating the visible and the infrared diffraction patterns that were reported in Ref. 9.

Short of obtaining flat SLMs, we may be able to achieve more-accurate calibrations by reducing coverglass and interface reflections (e.g., wedged glass, narrowband incoherent illumination, antireflective coating), increasing the backplane's reflectivity to greater its current ~50% level (to reduce contrast of coverglass reflections), and increasing the number of gray levels over the linear range of the liquid crystal (to reduce quantization errors).

This study was supported by U. S. Missile Defense Agency contract F19628-02-C-0083 through the U.S. Air Force.

References

1. Y. Zhisheng, L. Yulin, L. Jifang, and H. Zhengquan, "Measurement of the phase modulation of liquid-crystal televisions by a noninterferometric technique," Appl. Opt. **37,** 3069–3075 (1998).
2. N. Konforti, E. Marom, and S. T. Wu, "Phase-only modulation with twisted nematic liquid-crystal spatial light modulator," Opt. Lett. **13,** 251–253 (1988).
3. L. Goncalves Neto, D. Roberge, and Y. Sheng, "Programmable optical phase-mostly holograms with coupled-mode modulation liquid-crystal television," Appl. Opt. **34,** 1944–1950 (1995).
4. D. J. Cho, S. T. Thurman, J. T. Donner, and G. M. Morris, "Characteristics of a 128 × 128 liquid-crystal spatial light modulator for wave-front generation," Opt. Lett. **23,** 969–971 (1998).
5. H. K. Liu, J. A. Davis, and R. A. Lilly, "Optical-data-processing properties of a liquid-crystal television spatial light modulator," Opt. Lett. **10,** 635–637 (1985).
6. A. Bergeron, J. Gauvin, F. Gagnon, D. Gingras, H. H. Arsenault, and M. Doucet, "Phase calibration and applications of a liquid-crystal spatial light modulator," Appl. Opt. **34,** 5133–5139 (1995).
7. T. H. Barnes, T. Eiju, K. Matusda, and N. Ooyama, "Phase-only modulation using a twisted nematic liquid crystal television," Appl. Opt. **28,** 4845–4852 (1989).
8. J. L. de Bougrenet de la Tocnaye, and L. Dupont, "Complex amplitude modulation by use of liquid-crystal spatial light modulators," Appl. Opt. **36,** 1730–1741 (1997).
9. X. Xun, X. Chang, and R. W. Cohn, "System for demonstrating arbitrary multi-spot beam steering from spatial light modulators," Opt. Express **12,** 260–268 (2004), http://www.opticsexpress.org.
10. J. Stockley, S. Serati, X. Xun, and R. W. Cohn, "Liquid crystal spatial light modulator for multispot beam steering," in *Free Space Laser Communication and Active Laser Illumination III*, D. G. Voelz and J. C. Ricklin, eds., Proc. SPIE **5160,** 208–215 (2004).
11. Jay Stockley, Boulder Nonlinear Systems, Inc., 450 Courtney Way, Lafayatte, Colo. 80026 (personal communication, 2003).
12. D. Malacara, ed., *Optical Shop Testing*, 2nd ed. (Wiley, New York, 1992), Chap. 14, p. 501.
13. G. Newgebauer, R. Hauck, and O. Bryndahl, "Computer-generated circular carrier Fourier holograms," Opt. Commun. **48,** 89–92 (1983).
14. M. Duelli, M. Reece, and R. W. Cohn, "Modified minimum-distance criterion for blended random and nonrandom encoding," J. Opt. Soc. Am. A **16,** 2425–2438 (1999).